

Theory of spin and orbital charge conversion at the surface states of $\text{Bi}_{1-x}\text{Sb}_x$ topological insulator

Armando Pezo,¹ Jean-Marie George,¹ and Henri Jaffrès¹

¹Laboratoire Albert Fert, CNRS, Thales, Université Paris-Saclay, 91767, Palaiseau, France

(Dated: July 4, 2024)

Topological insulators are quantum materials involving Time-reversal protected surface states (TSS) making them appealing candidates for the design of next generation of highly efficient spintronic devices. The very recent observation of large transient spin-charge conversion (SCC) and subsequent powerful THz emission from $\text{Co|Bi}_{1-x}\text{Sb}_x$ bilayers clearly demonstrates such potentiality and feasibility for the near future. Amongst the exotic properties appearing in and at the surface of such quantum materials, spin-momentum locking (SML) and Rashba-Edelstein effects remain as key ingredients to effectively convert the spin degree of freedom into a charge or a voltage signal. In this work, we extend our analyses to the quantification of orbital momentum-locking and related orbital charge conversion effects in $\text{Bi}_{.85}\text{Sb}_{.15}$ via orbital Rashba-Edelstein effects. In that sense, we will provide some clear theoretical and numerical insights implemented by multi-orbital and multi-layered tight-binding methods (TB) to clarify our recent experimental results obtained by THz-TDS spectroscopy.

Theoretical proposals made almost two decades ago for exotic materials displaying an insulating bulk with metallic surface states [1, 2] led quickly to their experimental observation by measuring the spin Hall conductance in HgTe — CdTe quantum wells [3] and more recently in two-dimensional materials like bismuthene [4]. The strong spin-orbit coupling (SOC) in Bi-based materials makes them ideal candidates for spintronics and valleytronics applications [5–9] owing to the so-called band inversion mechanism responsible for the emergence of their topological properties. Among them, the Bulk-Boundary correspondence [10], relates their topological classification to the existence of spin-polarized surface states (TSS) [11] manifesting a strong spin momentum locking (SML) preventing back-scattering as long as disorder does not break heavily the time reversal symmetry (TRS) [12, 13]. In a couple of recent papers, it was successfully demonstrated by time-domain THz spectroscopy (THz-TDS) that Ag|Bi Rashba [14], Bi_2Se_3 [15] and SnBiTe TI [16] as well as $\text{Bi}_{1-x}\text{Sb}_x$ alloy family [17–20] enables robust spin-charge conversion (SCC) from 3d ferromagnetic (FM) injectors, proven to be as efficient as usual Pt or W heavy metals owing to the particular six-fold symmetry SML displayed by their TSS. Moreover, recent ab-initio calculations emphasize on the optical generation of orbital currents in BiAg_2 surface [21].

The rise of the orbital angular momentum (OAM) from electronic quasiparticles as a new degree of freedom has recently attracted much attention [22–24]. This is partly explained by the ability to generate a prominent OAM flow without the restricting requirement of a large SOC; and possibly largely exceeding the spin flow generated by Pt or W [25]. It was postulated that either the orbital Hall effect (OHE) or the orbital Rashba-Edelstein effect (OREE) may arise from the orbital texture in the bulk or from the orbital momentum locking (OML) at interfaces even involving centrosymmetric materials [26]. Conversely, the occurrence of a SML on the Fermi surface (FS) under SOC suggests a chiral OML texture,

as previously demonstrated by ARPES on Bi_2Se_3 [27], and possibly resulting in an orbital to charge conversion (OCC) phenomenon. These ingredients bring new avenues as it broadens the set of materials and also poses new challenges owing to the intrinsic entanglement with the spin degree of freedom. In this regard, one way to reduce the role of SOC is to use light materials as $\text{LaAlO}_3|\text{SrTiO}_3$ [28], $\text{KTaO}_3|\text{Al}$ [29], CuO_x [30] oxides or Co|Al [31] or Ni|Cu [32] metallic interfaces.

In this letter, we aim at disentangling both spin and orbital charge conversion (CC) processes in $\text{Bi}_{1-x}\text{Sb}_x$ TI known as a very efficient converter. In particular we explore quantitatively the different mechanisms into play among Hall effects arising from a specific Berry curvature or Rashba-Edelstein (RE) contributions, marking a difference between bulk and interfacial phenomena. We used a modified $\{s, p_x, p_y, p_z\} \otimes \{\uparrow, \downarrow\}$ sp^3 tight-binding (TB) multiband Hamiltonian [33] for Bi [34] developed for thin films and capturing our ARPES data [19, 35]. This approach was used to demonstrate how the non-trivial topological phase arises for a given Sb content x in a certain window [36, 37]. The electronic properties of the BiSb alloys are derived from the modified Virtual Crystal Approximation (VCA) [38] including adequate surface potential terms.

The respective spin (SHC) and orbital Hall conductivity (OHC) scaling the bulk contribution writes:

$$\sigma_{xy}^z = \frac{e^2 \hbar}{\Omega} \sum_{\mathbf{k}, n \neq m} \frac{\langle n, \mathbf{k} | \hat{v}_x | m, \mathbf{k} \rangle \langle m, \mathbf{k} | \hat{j}_y^z | n, \mathbf{k} \rangle}{(\varepsilon_m - \varepsilon_n)^2} f_{\mathbf{k}, n}, \quad (1)$$

where $\hat{j}_y^z = \frac{1}{2} \{ \hat{v}_y, \hat{O}_z \}$ is the angular momentum current, with $\hat{O}_z = \hat{s}_z, \hat{L}_z$ the respective spin and OAM operators oriented along \hat{z} , \hat{y} the flow direction of the angular momentum and \hat{v}_x the velocity operator directed along the electric field. We note $\hat{\sigma}_{x,y,z} = 2\hat{s}_{x,y,z}$ the corresponding

Pauli matrix. These are evaluated for electronic states $|n, \mathbf{k}\rangle$ of eigenvalues ε_n and $f_{\mathbf{k},n}$ is the Fermi-Dirac distribution, e and Ω are the electronic charge and unit cell volume respectively. Any circular permutation between $(\hat{x}, \hat{y}, \hat{z})$ in Eq.1 refers to a frame rotation.

Using Eq. 1 we have calculated both the SHC and OHC, displayed in Fig. 1, for pure Bi (a,b) and $\text{Bi}_{0.85}\text{Sb}_{0.15}$ in the topological phase window (c). First, in order to validate our bulk TB parametrization, we compare the intrinsic response for pure Bi obtained from density functional density (DFT) simulations using SIESTA for the self-consistent cycle and using *sisl* as a post-processing step (details in the SI.) (a) and from our TB bulk Hamiltonian (b). These intrinsic effects are observed to be in very close agreement with previous calculations [39] reaching however quite moderate values, typically $\simeq 500$ S/cm within the chosen energy window close to the Fermi level (FL) located at $E = 0$ (Fig. 1a,b). Three different components of the SHC tensor are displayed revealing the rhombohedral crystal anisotropy. Fig. 1c) displays the corresponding SHC $\text{Bi}_{0.85}\text{Sb}_{0.15}$ showing only moderate changes compared to pure Bi. We have extended our approach to the multi-layer slab geometry (see SI). Here, as for pure Bi layers [40], additional surface dipolar hopping terms and surface potential [19, 22, 35, 41], the so-called γ_{sp} and γ_{pp} terms in an sp^3 model [42], were determined from our ARPES data acquired on a 5 nm thick BiSb layer (Fig. 2a-b). Our present calculations on a 12 bilayers (BL) $\text{Bi}_{0.85}\text{Sb}_{0.15}$ (Fig. 1c) reveal that decreasing the BiSb layer thickness down to few BLs has a strong impact on the SHC in the bandgap region whatever the spin-injection direction. Two types of calculations have been performed this way: with (w/ straight lines) and without (wo/ dashed lines) additional surface hopping terms. A severe decrease of SHC for ultrathin films down to less than $\simeq 100 - 200$ S/cm around $E = 0$ originates from the changes in the electronic states at the surface and/or from quantization effects (owing to the $(\varepsilon_n - \varepsilon_n)$ increasing term in the denominator of Eq.1). Possibly, the top and bottom surfaces of opposite spin-chirality starts to mix together in the middle of the film leading to such severe SHC drop. We demonstrate then that SHC arising from evanescent TSS close to the gap can hardly drive efficient SCC. SHC can be partially recovered in the CB for propagating states in the conduction band (CB) where localization effects are strongly attenuated.

The extension of our TB theory to the OHC (see SI) shows that the latter ($\sigma_{OHE}^{\text{BiSb}} < 100$ S/cm) cannot explain the CC at the level of Pt with $\sigma_{SHE}^{\text{Pt}} \simeq 2500 - 3000$ S/cm [43] like observed in THz-TDS [19, 20]. Such conclusions of non dominant SHC and OHC are even more supported by the additional reduction of the SCC expected at small layer thickness when the spin-diffusion length $\lambda_{sf}^{\text{BiSb}}$ is typically larger than some units

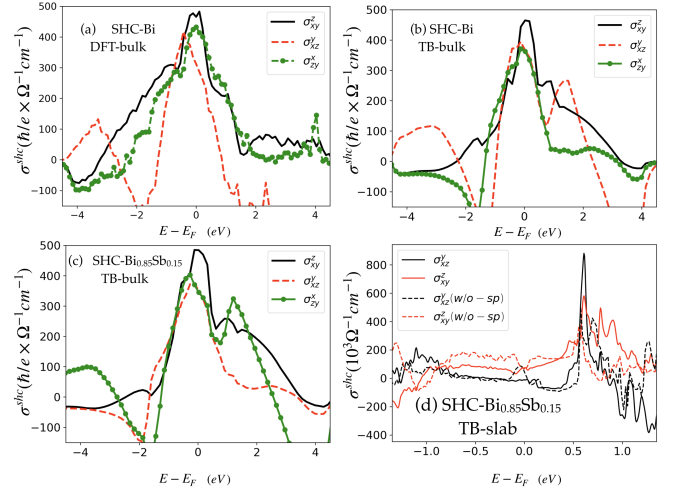


FIG. 1. SHC for bulk Bi (a,b). 3 components of the SHC tensor vs. E_F obtained respectively by DFT (a) and from TB (b). SHC for $\text{Bi}_{85}\text{Sb}_{15}$ showing only moderate changes compared to pure Bi. In (d) we show the SHC components calculated for a TB 12 BLs (5 nm) $\text{Bi}_{85}\text{Sb}_{15}$ slab geometry for respective in-plane (red) and out-of-plane (black) spin currents j^s . We considered bare BiSb surface (dashed) and surface hopping term corrections (solid) with opposite values for the two opposite surfaces. In order to match the TB model with ARPES, we considered on-site $s-p_z$ coupling $\gamma_{sp} = -0.2$ eV, surface hopping terms respectively equalling $\gamma_{sp1} = 0.3$ eV and $\gamma_{pp} = -0.6$ eV.

of nm [17] according to $\text{SCC} \propto \frac{(\mathcal{G}_{\uparrow\downarrow} r_s) \tanh^2 \left(\frac{t \text{BiSb}}{2\lambda_{sf}^{\text{BiSb}}} \right)}{1 + (\mathcal{G}_{\uparrow\downarrow} r_s) \coth \left(\frac{t \text{BiSb}}{\lambda_{sf}^{\text{BiSb}}} \right)} \propto \left(\frac{t \text{BiSb}}{2\lambda_{sf}^{\text{BiSb}}} \right)^2$ [19, 30] with t the layer thickness, r_s the spin resistance of BiSb and $\mathcal{G}_{\uparrow\downarrow}$ the spin-mixing conductance at Co|BiSb interfaces.

Eventually, CC occurring at interfaces may be better captured by Rashba-Edelstein effects (REE), where the inversion symmetry breaking may lead to angular momentum locking (spin or orbital). Either Hall effects or REE are usually attributed to different origins in terms of *interband* vs. *intra-band* quantum transitions. Those are complementary in various phenomena as the spin-orbit torque (SOT) and its reciprocal effect as orbital pumping in both ferromagnetic resonance (FMR) or THz regimes. iSREE mechanisms have been already tackled in our previous work on Co|BiSb giving a reliable contribution to the ultrafast SCC [19, 20]. A constant CC vs. layer thickness as observed was ascribed to the very short penetration of the TSS into the bulk in a sub-nanometric lengthscale. However, the missing ingredient is the inverse orbital REE (iOREE) evaluation.

Calculated spin and orbital polarized surface band structure corresponding to the first BL of a 12 BLs thick $\text{Bi}_{0.85}\text{Sb}_{0.15}$ ($\simeq 5$ nm) are shown in Fig. 2(c,e). Fig. 2c

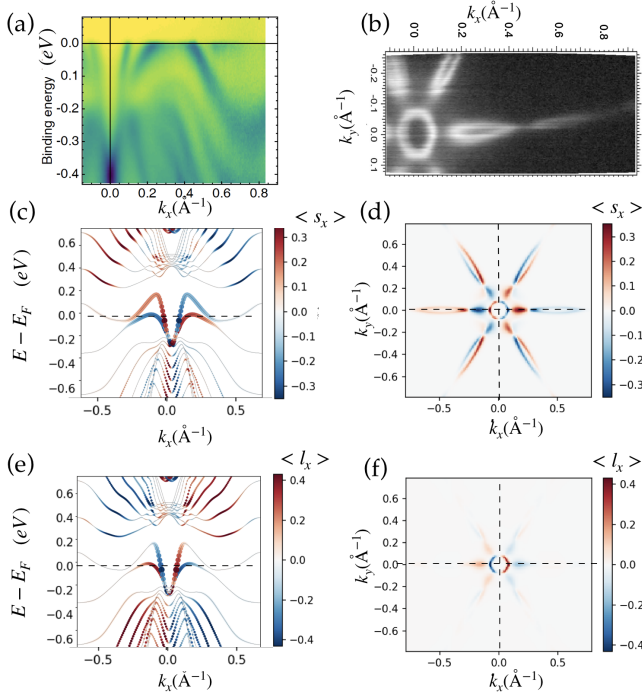


FIG. 2. (a) ARPES data (from Ref. [19]) acquired on a 5 nm (12 BLs) $\text{Bi}_{0.85}\text{Sb}_{0.15}$ film displaying electronic energy dispersion along the $\hat{x} = \bar{M} - \bar{\Gamma} - \bar{M}'$ line in the ($E = -0.4, 0$) eV energy window ($E = 0$ corresponds to the Fermi energy). (b) ARPES data of the 2D Fermi cut of the DOS. (c) and (e) TB calculation of the respective spin (σ_y) and orbital (L_y) DOS projection onto the first (1^{st}) BiSb BL along the same $\hat{x} = \bar{M} - \bar{\Gamma} - \bar{M}'$ high symmetry line. The bottom BL shows identical energy dispersion with opposite angular momentum chirality. (d-f) TB calculation of the Fermi surface 2D cuts of the \hat{y} component of respective spin and orbital resolved DOS projected onto the 1^{st} BL.

displays the spin-resolved σ_y DOS in the (k_x, E) space below the Fermi energy ($E = 0$) corresponding to the \hat{y} in-plane spin component oriented along $\bar{\Gamma} - \bar{K}$ for a wavevector \mathbf{k}_x along the $\hat{x} = \bar{M} - \bar{\Gamma} - \bar{M}'$ of the 2-dimensional (2D) Brillouin zone (BZ). We observe positive (red) and negative (blue) spin projections for the two surface states S_1 and S_2 crossing the Fermi energy. This witnesses the SML property with a maximum in-plane expected spin value $\langle \psi_{\mathbf{k},n} | \hat{\sigma}_y | \psi_{\mathbf{k},n} \rangle \simeq 0.3 \hbar$ in average [22], close to $\bar{\Gamma}$. The resulting spin-resolved Fermi cut within the BZ (Fig. 2d) reveals the peculiarity of the FS for Bi-based rhombohedral stacking made of: an almost circular central SML Rashba-like ring with two additional holes and electrons pockets away from $\bar{\Gamma}$ of hexagonal symmetry [44]. The ensemble of these TB calculations are compared with very good agreement to our (spin-)ARPES data (Figs 2a,b) [19, 35] displaying the energy dispersion (a) and Fermi cut of the DOS (b).

Extended analyses for the \hat{L}_y OAM in-plane orbital component is plotted on Fig. 2(e, f) in the same $(\mathbf{k}_x,$

energy) window. One observes clear features of OML with positive (red) and negative (blue) projections as for Bi_2Se_3 [27, 45]. Two main differences arise compared to the spin: *i*) the orbit is polarized (locked) in the opposite direction in agreement with Ref. [22] *ii*) the orbital expectation value is larger ($\langle \psi_{\mathbf{k},n} | \hat{L}_y | \psi_{\mathbf{k},n} \rangle \simeq 0.4 \hbar$) than the spin one in average, in the range of values for BiAg_2 given by Ref. [22]. The resulting in plane orbital-resolved Fermi cut in the BZ is plotted on Fig. 2(c) emphasizing the relevance of the orbital polarization of the electron pocket near $\bar{\Gamma}$.

We turn to the evaluation of spin and orbital iREE at the top surface and compare the two. To that end, we generalize the expression of the REE length [29, 46, 47], $\Lambda_{xy}^{\text{iREE}}$ obtained from a refined linear response theory [19] and whose methodology is given in (SI):

$$\Lambda_{xy}^{\text{iREE}} = \frac{\sum_{n,\mathbf{k}} \partial_{E_{n,\mathbf{k}}} f_{n,\mathbf{k}} \langle n, \mathbf{k} | \hat{v}_x \tau_0 | n, \mathbf{k} \rangle \langle n, \mathbf{k} | \hat{\Pi}_y | n, \mathbf{k} \rangle}{\sum_{n,\mathbf{k}} \partial_{E_{n,\mathbf{k}}} f_{n,\mathbf{k}}}, \quad (2)$$

with $\hat{\Pi}_y$ the *intra-band* angular momentum projector of the impinging out-of equilibrium polarized carriers onto the TI electronic states (n, \mathbf{k}) projected onto the first BL only, owing to the strong localization of the TSS. $\Lambda_{xy}^{\text{iREE}}$ is weighted by the derivative of the Fermi distribution function $\partial_{E_{n,\mathbf{k}}} f_{n,\mathbf{k}} = \delta(E - \epsilon_{k,n})$ that is the local DOS. Such expression for $\Lambda_{xy}^{\text{iREE}}$ is derived by considering the \mathbf{k} dependence of the scattering rate on the FS related to both the spin and orbital momentum locking according to $\tau(\mathbf{k}) = \tau_0 / \langle \sigma_y \rangle_{\mathbf{k},n}^2$. This reflects the anisotropy of decoherence over the FS with τ_0 the angular averaged scattering time.

We note \hat{y} the quantization axis along the magnetization of the injector. The $\hat{\Pi}_y$ projector in Eq. 2 writes generally $\hat{\Pi} = \sum_m \varrho_m |m = \mu \otimes s\rangle \langle m = \mu \otimes s|$ where $|m\rangle$ are the incoming electronic states of density matrix ϱ_m containing both spin (s) and orbital (μ) characters. We note $(\varrho_{\uparrow} - \varrho_{\downarrow}) = \mathcal{M}_s$ and $(\varrho_{+1} - \varrho_{-1}) = \mathcal{M}_l$ the spin and orbital accumulation (densities). For the spin only case $\hat{\Pi}_s = \frac{1}{2}(\varrho_{\uparrow} + \varrho_{\downarrow}) \hat{L}_{2 \times 2} + \frac{1}{2}(\varrho_{\uparrow} - \varrho_{\downarrow}) \hat{\sigma}_y$, showing that the non-vanishing spin matrix element of $\langle n, \mathbf{k} | \hat{v}_x \tau | n, \mathbf{k} \rangle \langle n, \mathbf{k} | \hat{\Pi}_y | n, \mathbf{k} \rangle$ in Eq. 2, symmetric in \mathbf{k} , only retains the $(\varrho_{\uparrow} - \varrho_{\downarrow}) \hat{\sigma}_y = \mathcal{M}_s \hat{\sigma}_y$ term as expected.

In order to include the OAM, we first consider *uncorrelated* spin and orbital degrees of freedom and we are left with $\hat{\Pi} = \hat{\Pi}_s \otimes \hat{\Pi}_L = (\varrho_s |s\rangle \langle s|) \otimes (\varrho_\mu |\mu\rangle \langle \mu|)$ [27] ($|\mu\rangle \langle \mu| = \hat{\pi}_\mu$ are the orbital projector onto $\mu = \pm 1, 0$ [21, 22]). $\hat{\pi}_{\pm 1} = |l_y = \pm 1\rangle \langle l_y = \pm 1|$ projects onto the orbital angular momentum along the in-plane \hat{y} direction with respective ± 1 eigenvalues whereas $\hat{\pi}_0$ projects onto the p_y orbital ($\hat{\pi}_0 = |l_y = 0\rangle \langle l_y = 0|$) with:

$$\hat{\pi}_{\pm 1} = \frac{\pm \hat{L}_y}{2} (\hat{I} \pm \hat{L}_y) \quad ; \quad \hat{\pi}_0 = \hat{I} - \hat{L}_y^2, \quad (3)$$

acting on the TI states $|n\rangle$. The charge current response to the incoming total angular momentum flow reads $\mathcal{J}_c \propto \Sigma_{\mathbf{k},n} \langle \mathbf{k}, n | \hat{v}_x | \mathbf{k}, n \rangle \times \left(\varrho_s \langle \mathbf{k}, n | \hat{\Pi}_s | \mathbf{k}, n \rangle \right) \times (\varrho_\mu \langle \mathbf{k}, n | \hat{\pi}_\mu | \mathbf{k}, n \rangle)$. One easily checks that $\hat{L}_y = \hat{\pi}_{+1} - \hat{\pi}_{-1}$ in Eq. 2 required for the determination of the iOREE. We also see that $\hat{L}_y^2 = \hat{\pi}_{+1} + \hat{\pi}_{-1}$ and $\hat{\pi}_{-1} + \hat{\pi}_0 + \hat{\pi}_1 = \hat{I}$ the unity matrix.

Non-magnetic TI and TRS: Because $\langle \mathbf{k}, n | \hat{v}_x | \mathbf{k}, n \rangle$ is asymmetric in \mathbf{k} upon TRS, there exists 3 different mechanisms to the CC: *i)* a pure spin-contribution giving rise to iSREE because $\langle \hat{\sigma}_y \rangle_{\mathbf{k},n}$ is asymmetric in \mathbf{k} , *ii)* a pure orbital contribution (iOREE) owing to that $\langle \hat{\pi}_{-1} \rangle_{\mathbf{k}} = -\langle \hat{\pi}_{-1} \rangle_{-\mathbf{k}} = -\langle \hat{\pi}_{+1} \rangle_{\mathbf{k}}$ is also asymmetric in \mathbf{k} upon TRS, and *iii)* an entangled spin-orbital contribution originating from the $\langle \mathbf{k}, n | \left(\hat{\pi}_0 - \frac{\hat{L}_y^2}{2} \right) \hat{\sigma}_y | \mathbf{k}, n \rangle = \langle \mathbf{k}, n | \left(\hat{I} - \frac{3}{2} \hat{L}_y^2 \right) \hat{\sigma}_y | \mathbf{k}, n \rangle$ term (see SI). Note that $\langle L_y^2 \rangle = \frac{2}{3}$ for no net orbital polarization.

i) Case of unpolarized orbital: $\varrho_{+1} = \varrho_{-1} = \varrho_0$. This is the pure spin iSREE from spin-polarized carriers of polarisation \mathcal{M}_s impinging the BiSb surface and generated by RF or laser spin pump. $\hat{\Pi}_y = \hat{\sigma}_y$ in Eq. 2 the analytical form given in Refs. [19, 47] is recovered. Our TB calculations of the iSREE length (Λ_{xy}^{iSREE}) for a scattering time $\tau_0 = 10$ fs are shown on Fig. 3a, for two different $\text{Bi}_{0.85}\text{Sb}_{0.15}$ thicknesses (6 and 12 BLs). The typical $\Lambda_{xy}^{SREE} \approx 0.2$ nm calculated near E_F ($E = 0$) approaches the $(\theta_{SHE}^{Pt} \times \lambda_{sf}^{Pt})$ product for Pt [43] giving its SCC efficiency in the same length unit. The relative lack of variation of Λ_{xy}^{iSREE} on the layer thickness [19] can be explained by the short evanescent length of the surface states (TSS) in BiSb [19, 35] as for Bi [48]. This feature is exemplified in the inset of Fig. 3a showing the localisation of Λ_{xy}^{iSREE} at the surface over only 2 BLs.

ii) Case of polarized orbital involving circular OAM: $\varrho_{+1} \neq \varrho_{-1}$ with $\mathcal{M}_l = (\varrho_{+1} - \varrho_{-1})$ the incoming OAM accumulation and $\mathcal{M}_s = 0$ (no spin). We then use $\langle \hat{\pi}_{+1} \rangle_{\mathbf{k}} = -\langle \hat{\pi}_{-1} \rangle_{\mathbf{k}}$ and $\langle \hat{\pi}_{+1} \rangle_{\mathbf{k}} - \langle \hat{\pi}_{-1} \rangle_{\mathbf{k}} = \langle \hat{L}_y \rangle_{\mathbf{k}}$ in Eq. 2.

The orbital REE length, Λ_{xy}^{iOREE} , admits about the same value ($\Lambda_{xy}^{iOREE} \approx 0.05$ nm) than the spin in the bandgap at $E_F = 0$ in Fig. 3(a) with the same typical evanescent length (inset of Fig. 3a), also at the level of the Pt SCC efficiency. This gives rise to an additive contribution to the SCC (same sign) at the FL. We also observe that the spin and orbital textures are opposite within the energy windows depicted in Fig. 2. This difference between spin and orbital behaviour is related to a different partition of the two S_1 and S_2 surface states *iREE*. The comparison between spin and orbital responses are even more exemplified near the CB at higher energy ($E = 0.2$ eV), where the orbital response is larger than the spin one, with now an opposite sign.

The orbital response appears to be even more robust

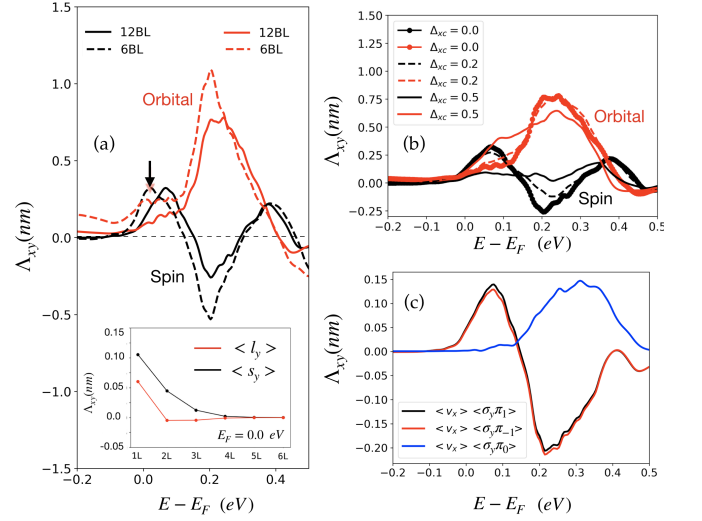


FIG. 3. iREE(a) for spin and orbital degrees of freedom displaying the calculated Λ_{xy}^{iREE} in nm for 6 (dashed lines) and 12 (solid lines) BLs $\text{Bi}_{0.85}\text{Sb}_{0.15}$. The inset shows the decay within each BL for the spin (black) and orbital (red) curves onto the TSS calculated at the Fermi level remarked by the vertical arrow. In (b) we show the same response in the case of an in-plane contact exchange of 0.2 (dashed) and 0.5 eV (dashed-point) The CC projected onto $\pi_{\pm 1}$ and π_0 for 12 BLs (without exchange) are shown in (c). Given that all three projections Π sum up the unity, the total contribution equals of the straight black curve in (a).

than the spin over a large energy window (in the typical 0-0.3 eV range as generated by a short laser excitation [49]), because of preserving the same CC sign over the whole energy range. Such conclusion has nevertheless to be moderated: an linear-polarized optical excitation mainly generates spins, with subsequent OAM obtained from perturbation introduced by SOC [21]. Also, the condition, not discussed here, is the absence of any decoherence process between excitation and relaxation onto the TSS. The case of correlated spin-orbital variables is made possible by the spin-orbit interactions acting in the FM reservoir. This yields a same qualitative expression for the iOREE which amplitude is now scaled by the $\mathcal{M}_s \mathcal{P}_l$ product with \mathcal{P}_l the orbital polarization under spin-orbit strength instead of \mathcal{M}_l for uncorrelated spin and orbital states (SI).

iii) Case of linear polarized orbital with $2\varrho_0 \neq (\varrho_{+1} + \varrho_{-1})$. Now, a pure linear orbitally polarized carriers is described by the $\hat{\pi}_y = \langle \mathbf{k}, n | \left(\hat{I} - \hat{L}_y^2 \right) \hat{\sigma}_y | \mathbf{k}, n \rangle$ term and whose result is plotted on Fig. 3c (blue line). Such spin-orbital response is small in the bandgap and larger in the CB region. It originates from the OML and localization of the wavefunctions on the TSS projecting along the $l_y = \pm 1$ values forbidding thus the coupling to $l_y = 0$ states. The propagating Bloch states are recovered in the CB partly releasing possible coupling with linear orbital $l_y = 0$ states. The perfect overlap between

$\langle \hat{\pi}_{\pm} \rangle \hat{\sigma}_y$ response in the absence of exchange (red and black curves on Fig. 3c explains the cancellation of such term for circularly orbital polarized carriers.

Case of proximity exchange Δ_{exc} by contact with the 3d FM: TRS breaking. Among the various other additional terms to the SCC due to the TRS breaking, we have evaluated the respective spin and orbital iREE response by introducing an additional *contact* exchange term $\hat{\mathcal{H}} = -\Delta_{exc} \hat{m} \cdot \hat{\sigma}$ acting on the TSS over a typical localization length of 2 BLs. The calculations have been performed for typical values $\Delta_{exc} = 0.2, 0.5$ eV. The results (Fig. 3b) show that, although the spin response (iSREE) is largely altered for $\Delta_{exc} = 0.5$ eV (however kept still quite large for $\Delta_{exc} = 0.2$ eV), the orbital response (iOREE) remains almost unaffected by such contact exchange interactions.

In summary, we have described the anatomy of respective spin and orbital-to-charge conversion in $\text{Bi}_{1-x}\text{Sb}_x$ TIs. By extending the analysis of the spin transport to the orbital peculiarities, we were able to quantify both bulk spin and orbital contributions to the iS(O)HE, pointing out the small values of the total response.

We therefore provide a detailed analysis of the Rashba-Edelstein effect (REE) arising from both degrees of freedom. In the latter case, we disentangle the orbital contributions that lead to charge conversion such that, in terms of both circular and linear orbital polarization projectors. Such a decomposition allowed us to enhance a pure orbital part arising when such symmetry is broken by an in-plane magnetic exchange field. The use of orbital ferromagnetic injectors like played by Ni [32, 50] or CoPt [51] alloys may be used to probe the OCC with BiSb materials.

ACKNOWLEDGMENTS

The authors acknowledge P. Le Fèvre (Soleil Synchrotron, Saint-Aubin, France) and L. Baringthon for their help in the ARPES measurements. This study has been supported by the French National Research Agency under the project 'ORION' ANR-20-CE30-0022-02, the project 'DYNTOP' ANR-22-CE30-0026 and by a France 2030 government grant managed by the French National Research Agency PEPR SPIN ANR-22-EXSP0009 (SPINTHEORY).

-
- [1] C. L. Kane and E. J. Mele, "Quantum spin hall effect in graphene," *Phys. Rev. Lett.* **95**, 226801 (2005).
 - [2] B. Andrei Bernevig, Taylor L. Hughes, and Shou-Cheng Zhang, "Quantum spin hall effect and topological phase transition in hgte quantum wells," *Science* **314**, 1757–1761 (2006).
 - [3] Markus König, Steffen Wiedmann, Christoph Brüne, Andreas Roth, Hartmut Buhmann, Laurens W. Molenkamp, Xiao-Liang Qi, and Shou-Cheng Zhang, "Quantum spin hall insulator state in hgte quantum wells," *Science* **318**, 766–770 (2007).
 - [4] F. Reis, G. Li, L. Dudy, M. Bauernfeind, S. Glass, W. Hanke, R. Thomale, J. Schäfer, and R. Claessen, "Bismuthene on a SiC substrate: A candidate for a high-temperature quantum spin hall material," *Science* **357**, 287–290 (2017).
 - [5] Wei xiao Ji, Chang wen Zhang, Meng Ding, Bao min Zhang, Ping Li, Feng Li, Miao juan Ren, Pei ji Wang, Run wu Zhang, Shu jun Hu, and Shi shen Yan, "Giant gap quantum spin hall effect and valley-polarized quantum anomalous hall effect in cyanided bismuth bilayers," *New J. Phys.* **18**, 083002 (2016).
 - [6] Lu Lu, Zhiming Liang, Leiming Wu, YunXiang Chen, Yufeng Song, Sathish Chander Dhanabalan, Joice Sophia Ponraj, Biqin Dong, Yuanjiang Xiang, Feng Xing, Dianyuan Fan, and Han Zhang, "Few-layer bismuthene: Sonochemical exfoliation, nonlinear optics and applications for ultrafast photonics with enhanced stability," *Laser Photonics Rev.* **12**, 1700221 (2017).
 - [7] Shengli Zhang, Meiqiu Xie, Fengyu Li, Zhong Yan, Yafei Li, Erjun Kan, Wei Liu, Zhongfang Chen, and Haibo Zeng, "Semiconducting group 15 monolayers: A broad range of band gaps and high carrier mobilities," *Angew. Chem., Int. Ed.* **55**, 1666–1669 (2015).
 - [8] Ming-Yang Liu, Yang Huang, Qing-Yuan Chen, Ze-Yu Li, Chao Cao, and Yao He, "Strain and electric field tunable electronic structure of buckled bismuthene," *RSC Adv.* **7**, 39546–39555 (2017).
 - [9] Xiaoxiong Wang, Guang Bian, Caizhi Xu, Peng Wang, Huanzhi Hu, Weiping Zhou, S A Brown, and T-C Chiang, "Topological phases in double layers of bismuthene and antimonene," *Nanotechnology* **28**, 395706 (2017).
 - [10] Andrew M. Essin and Victor Gurarie, "Bulk-boundary correspondence of topological insulators from their respective green's functions," *Phys. Rev. B* **84**, 125132 (2011).
 - [11] C. L. Kane and E. J. Mele, " Z_2 topological order and the quantum spin hall effect," *Phys. Rev. Lett.* **95**, 146802 (2005).
 - [12] Armando Pezo, Bruno Focassio, Gabriel R. Schleder, Marcio Costa, Caio Lewenkopf, and Adalberto Fazzio, "Disorder effects of vacancies on the electronic transport properties of realistic topological insulator nanoribbons: The case of bismuthene," *Phys. Rev. Materials* **5**, 014204 (2021).
 - [13] Armando Pezo, Felipe Crasto de Lima, and Adalberto Fazzio, "Electronic and spin transport in bismuthene with magnetic impurities," *Solid State Communications* **376**, 115358 (2023).
 - [14] Matthias B. Jungfleisch, Qi Zhang, Wei Zhang, John E. Pearson, Richard D. Schaller, Haidan Wen, and Axel Hoffmann, "Control of terahertz emission by ultrafast spin-charge current conversion at rashba interfaces," *Phys. Rev. Lett.* **120**, 207207 (2018).

- [15] Xinbo Wang, Liang Cheng, Dapeng Zhu, Yang Wu, Mengji Chen, Yi Wang, Daming Zhao, Chris B. Boothroyd, Yeng Ming Lam, Jian-Xin Zhu, Marco Battiato, Justin C. W. Song, Hyunsoo Yang, and Elbert E. M. Chia, “Ultrafast spin-to-charge conversion at the surface of topological insulator thin films,” *Advanced Materials* **30**, 1802356 (2018).
- [16] E. Rongione, S. Fragkos, L. Baringthon, J. Hawecker, E. Xenogiannopoulou, P. Tsipas, C. Song, M. Micica, J. Mangeney, J. Tignon, T. Boulier, N. Reyren, R. Lebrun, J.-M. George, P. Le Fèvre, S. Dhillon, A. Dimoulas, and H. Jaffrès, “Ultrafast spin-charge conversion at $\text{snbi}_2\text{te}_4/\text{co}$ topological insulator interfaces probed by terahertz emission spectroscopy,” *Advanced Optical Materials* **10**, 2102061 (2022).
- [17] Vinay Sharma, Weipeng Wu, Prabesh Bajracharya, Duy Quang To, Anthony Johnson, Anderson Janotti, Garnett W. Bryant, Lars Gundlach, M. Benjamin Jungfleisch, and Ramesh C. Budhani, “Light and microwave driven spin pumping across fegab-bisb interface,” *Phys. Rev. Mater.* **5**, 124410 (2021).
- [18] Hanbum Park, Seungwon Rho, Jonghoon Kim, Hyeonmun Kim, Dajung Kim, Chul Kang, and Mann-Ho Cho, “Topological surface-dominated spintronic thz emission in topologically nontrivial $\text{bi}_{1-x}\text{sb}_x$ films,” *Advanced Science* **9**, 2200948 (2022).
- [19] E. Rongione, L. Baringthon, D. She, G. Patriarche, R. Lebrun, A. Lemaître, M. Morassi, N. Reyren, M. Mićica, J. Mangeney, J. Tignon, F. Bertran, S. Dhillon, P. Le Fèvre, H. Jaffrès, and J.-M. George, “Spin-momentum locking and ultrafast spin-charge conversion in ultrathin epitaxial $\text{bi}_{1-x}\text{sb}_x$ topological insulator,” *Advanced Science* **10** (2023), 10.1002/advs.202301124.
- [20] Seungwon Rho, Hanbum Park, Jeehong Park, Kwangsik Jeong, Hyeonmun Kim, Seok-Bo Hong, Jonghoon Kim, Hyeon Wook Lim, Yeonjin Yi, Chul Kang, and Mann-Ho Cho, “Exceptional spin-to-charge conversion in selective band topology of $\text{bi}/\text{bi}_{1-x}\text{sb}_x$ with spintronic singularity,” *Advanced Functional Materials* **33**, 2300175 (2023).
- [21] T. Adamantopoulos, M. Merte, D. Go, F. Freimuth, S. Blügel, and Y. Mokrousov, “Orbital rashba effect as a platform for robust orbital photocurrents,” *Phys. Rev. Lett.* **132**, 076901 (2024).
- [22] Dongwook Go, Jan-Philipp Hanke, Patrick M. Buhl, Frank Freimuth, Gustav Bihlmayer, Hyun-Woo Lee, Yuriy Mokrousov, and Stefan Blügel, “Toward surface orbitronics: giant orbital magnetism from the orbital rashba effect at the surface of sp-metals,” *Scientific Reports* **7**, 46742 (2017).
- [23] Dongwook Go, Daegeun Jo, Changyoung Kim, and Hyun-Woo Lee, “Intrinsic spin and orbital hall effects from orbital texture,” *Phys. Rev. Lett.* **121**, 086602 (2018).
- [24] Armando Pezo, Diego García Ovalle, and Aurélien Manchon, “Orbital hall effect in crystals: Interatomic versus intra-atomic contributions,” *Phys. Rev. B* **106**, 104414 (2022).
- [25] T. Tanaka, H. Kontani, M. Naito, T. Naito, D. S. Hirashima, K. Yamada, and J. Inoue, “Intrinsic spin hall effect and orbital hall effect in $4d$ and $5d$ transition metals,” *Phys. Rev. B* **77**, 165117 (2008).
- [26] Dongwook Go, Daegeun Jo, Changyoung Kim, and Hyun-Woo Lee, “Intrinsic spin and orbital hall effects from orbital texture,” *Phys. Rev. Lett.* **121**, 086602 (2018).
- [27] Seung Ryong Park, Jinhee Han, Chul Kim, Yoon Young Koh, Changyoung Kim, Hyungjun Lee, Hyoung Joon Choi, Jung Hoon Han, Kyung Dong Lee, Nam Jung Hur, Masashi Arita, Kenya Shimada, Hirofumi Namatame, and Masaki Taniguchi, “Chiral orbital-angular momentum in the surface states of bi_2se_3 ,” *Phys. Rev. Lett.* **108**, 046805 (2012).
- [28] Anas El Hamdi, Jean-Yves Chauleau, Margherita Boselli, Clémentine Thibault, Cosimo Gorini, Alexander Smogunov, Cyrille Barreateau, Stefano Gariglio, Jean-Marc Triscone, and Michel Viret, “Observation of the orbital inverse rashba-edelstein effect,” *Nature Physics* **19**, 1855–1860 (2023).
- [29] Sara Varotto, Annika Johansson, Borge Gobel, Luis M. Vicente-Arche, Sriyani Mallik, Julien Bréhin, Raphaël Salazar, François Bertran, Patrick Le Fèvre, Nicolas Bergeal, Julien Rault, Ingrid Mertig, and Manuel Bibes, “Direct visualization of rashba-split bands and spin/orbital-charge interconversion at ktao_3 interfaces,” *Nature Communications* **13**, 6165 (2022).
- [30] S. Krishnia, B. Bony, E. Rongione, L. Moreno Vicente-Arche, T. Denneulin, A. Pezo, Y. Lu, R. E. Dunin-Borkowski, S. Collin, A. Fert, J.-M. George, N. Reyren, V. Cros, and H. Jaffres, “Quantifying the large contribution from orbital Rashba-Edelstein effect to the effective damping-like torque on magnetization,” *APL Materials* **12**, 051105 (2024), https://pubs.aip.org/aip/apm/article-pdf/doi/10.1063/5.0198970/19918228/051105_1.5.0198970.pdf.
- [31] Sachin Krishnia, Yanis Sassi, Fernando Ajejas, Nicolas Sebe, Nicolas Reyren, Sophie Collin, Thibaud Denneulin, Andrès Kovacs, Rafal E. Dunin-Borkowski, Albert Fert, Jean-Marie George, Vincent Cros, and Henri Jaffrès, “Large interfacial rashba interaction generating strong spin-orbit torques in atomically thin metallic heterostructures,” *Nano Letters* **23**, 6785–6791 (2023).
- [32] Yong Xu, Fan Zhang, Albert Fert, Henri-Yves Jaffres, Yongshan Liu, Renyou Xu, Yuhao Jiang, Houyi Cheng, and Weisheng Zhao, “Orbitronics: light-induced orbital currents in ni studied by terahertz emission experiments,” *Nature Communications* **15**, 2043 (2024).
- [33] Yi Liu and Roland E. Allen, “Electronic structure of the semimetals bi and sb,” *Phys. Rev. B* **52**, 1566–1577 (1995).
- [34] Ph. Hofmann, “The surfaces of bismuth: Structural and electronic properties,” *Progress in Surface Science* **81**, 191–245 (2006).
- [35] Laëticia Baringthon, Thi Huong Dang, Henri Jaffrès, Nicolas Reyren, Jean-Marie George, Martina Morassi, Gilles Patriarche, Aristide Lemaître, François Bertran, and Patrick Le Fèvre, “Topological surface states in ultrathin $\text{bi}_{1-x}\text{sb}_x$ layers,” *Phys. Rev. Mater.* **6**, 074204 (2022).
- [36] B. Lenoir, H. Scherrer, and T. Caillat, “Chapter 4 an overview of recent developments for bisb alloys,” in *Recent Trends in Thermoelectric Materials Research I*, Semiconductors and Semimetals, Vol. 69, edited by Terry M. Tritt (Elsevier, 2001) pp. 101–137.
- [37] Jeffrey C. Y. Teo, Liang Fu, and C. L. Kane, “Surface states and topological invariants in three-dimensional topological insulators: Application to $\text{bi}_{1-x}\text{sb}_x$,” *Phys. Rev. B* **78**, 045426 (2008).

- [38] Hai-Jun Zhang, Chao-Xing Liu, Xiao-Liang Qi, Xiao-Yu Deng, Xi Dai, Shou-Cheng Zhang, and Zhong Fang, “Electronic structures and surface states of the topological insulator $\text{Bi}_{1-x}\text{Sb}_x$,” *Phys. Rev. B* **80**, 085307 (2009).
- [39] Cüneyt Şahin and Michael E. Flatté, “Tunable giant spin hall conductivities in a strong spin-orbit semimetal: $\text{Bi}_{1-x}\text{Sb}_x$,” *Phys. Rev. Lett.* **114**, 107201 (2015).
- [40] Kazuo Saito, Hirokatsu Sawahata, Takashi Komine, and Tomosuke Aono, “Tight-binding theory of surface spin states on bismuth thin films,” *Phys. Rev. B* **93**, 041301 (2016).
- [41] Jisook Hong, Jun-Won Rhim, Changyoung Kim, Seung Ryong Park, and Ji Hoon Shim, “Quantitative analysis on electric dipole energy in rashba band splitting,” *Scientific Reports* **5**, 13488 (2015).
- [42] Christian R. Ast and Isabella Gierz, “*sp*-band tight-binding model for the bychkov-rashba effect in a two-dimensional electron system including nearest-neighbor contributions from an electric field,” *Phys. Rev. B* **86**, 085105 (2012).
- [43] J.-C. Rojas-Sánchez, N. Reyren, P. Laczkowski, W. Savero, J.-P. Attané, C. Deranlot, M. Jamet, J.-M. George, L. Vila, and H. Jaffrès, “Spin pumping and inverse spin hall effect in platinum: The essential role of spin-memory loss at metallic interfaces,” *Phys. Rev. Lett.* **112**, 106602 (2014).
- [44] Hadj M. Benia, Carola Straßer, Klaus Kern, and Christian R. Ast, “Surface band structure of $\text{Bi}_{1-x}\text{Sb}_x(111)$,” *Phys. Rev. B* **91**, 161406 (2015).
- [45] Haijun Zhang, Chao-Xing Liu, and Shou-Cheng Zhang, “Spin-orbital texture in topological insulators,” *Phys. Rev. Lett.* **111**, 066801 (2013).
- [46] J. C. Rojas Sanchez, L. Vila, G. Desfonds, S. Gambarelli, Attané J. P., J. M. De Teresa, C. Magen, and A. Fert, “Spin-to-charge conversion using rashba coupling at the interface between non-magnetic materials,” *Nature Communications* **4**, 2944 (2013).
- [47] Annika Johansson, Börge Göbel, Jürgen Henk, Manuel Bibes, and Ingrid Mertig, “Spin and orbital edelstein effects in a two-dimensional electron gas: Theory and application to SrTiO_3 interfaces,” *Phys. Rev. Res.* **3**, 013275 (2021).
- [48] H Ishida, “Decay length of surface-state wave functions on $\text{Bi}(111)$,” *Journal of Physics: Condensed Matter* **29**, 015002 (2016).
- [49] Reza Rouzegar, Liane Brandt, Lukáš Nádvořník, David A. Reiss, Alexander L. Chekhov, Oliver Gueckstock, Chihun In, Martin Wolf, Tom S. Seifert, Piet W. Brouwer, Georg Woltersdorf, and Tobias Kampfrath, “Laser-induced terahertz spin transport in magnetic nanostructures arises from the same force as ultrafast demagnetization,” *Phys. Rev. B* **106**, 144427 (2022).
- [50] Tom S. Seifert, Dongwook Go, Hiroki Hayashi, Reza Rouzegar, Frank Freimuth, Kazuya Ando, Yuriy Mokrousov, and Tobias Kampfrath, “Time-domain observation of ballistic orbital-angular-momentum currents with giant relaxation length in tungsten,” *Nature Nanotechnology* **18**, 1132–1138 (2023).
- [51] Yongshan Liu, Yong Xu, Albert Fert, Henri-Yves Jaffrès, Sylvain Eimer, Tianxiao Nie, Xiaoqiang Zhang, and Weisheng Zhao, “Efficient terahertz generation from copt-based terahertz emitters via orbital-to-charge conversion,” (2024), [arXiv:2402.09228](https://arxiv.org/abs/2402.09228) [cond-mat.mes-hall].